Thermal Performance of Flat Micro Heat Pipe with Converging Microchannels

Gyoko Nagayama[a]*, Shunya Gyotoku[b], and Takaharu Tsuruta[a]

[a] Department of Mechanical Engineering, Kyushu Institute of Technology

1-1 Sensui, Tobata, Kitakyushu, Fukuoka 804-8550, Japan

[b] Graduate School of Engineering, Kyushu Institute of Technology

1-1 Sensui, Tobata, Kitakyushu, Fukuoka 804-8550, Japan

Abstract

Optimizing the groove size of flat micro heat pipes is crucial for improving their thermal performance. In this study, we developed a grooved converging microchannel array for use in a flat micro heat pipe to enhance the capillary force. A simplified theoretical analysis was used to optimize the groove size for given operating conditions of converging microchannels and straight microchannels. The evaporation section of the grooved microchannel was hydrophilic and had a smaller hydraulic diameter than the hydrophobic condensation section. The smaller diameter of the evaporation section enabled the condensed working fluid to be effectively drawn back to the same section. Experiments were performed to measure the thermal performance of the micro heat pipes under the analyzed operating conditions. Compared to a heat pipe with a straight microchannel, and a heat pipe with an unoptimized converging microchannel, the micro heat pipe with the optimized converging microchannel was confirmed to yield a higher thermal performance. Capillary-driven flow experiments at room temperature and atmospheric pressure were also used to investigate the capillary forces of the different microchannels. The optimized converging microchannel was once again observed to generate the largest capillary force.

Keywords: Converging microchannel, Micro heat pipe, Capillary force, Capillary-driven flow, Evaporation, Condensation

* Corresponding author. Tel.: +81 93 884 3139; Fax: +81 93 884 3139.
Email: nagayama@mech.kyutech.ac.jp (G. Nagayama)

Nomenclature

A	area, m^2
A_l	cross-sectional area of vapor, m^2
h	heat transfer coefficient, $W/(m^2 \cdot K)$
h_{fg}	latent heat, J/kg
H	groove height, m
N	number of grooves, -
L	length, m
$\dot{m}$	mass flow rate, kg/s
p	pressure, N/m^2
Q	input heat, W
R	thermal resistance, K/W
t	time, s
T	temperature, K
u	velocity, m/s
W	groove width, m

Greek Symbols

θ	contact angle, degree
λ	thermal conductivity, $W/(m \cdot K)$
μ	viscosity, $Pa \cdot s$
ρ	density, kg/m^3
σ	surface tension, N/m

Subscripts

c	condenser section
ca	capillary

e evaporator section

hp heat pipe

i liquid–vapor interface

l liquid

v vapor

1. Introduction

Micro heat pipes (MHPs) are self-driven cooling devices used for the removal of high heat flux from electronic devices. They can be fabricated using micro-electro-mechanical system (MEMS) technology, and considerable research has been channeled toward developing innovative MEMS-based flat micro heat pipes [1-20]. Although the compactness of flat MHPs is well-suited to the cooling of current and future chips, their thermal performance is limited by miniaturization. To improve the thermal performance of flat MHPs, a better understanding of the associated heat and mass transfer phenomena is required.

The capillary limit is a major challenge in improving the thermal performance of a flat MHP and avoiding dry-out in its evaporation section. In a flat MHP, the liquid returns from the condenser to the evaporator through a capillary structure that is usually composed of a microchannel array, which differs from the additional wicks installed in a conventional heat pipe. Accordingly, the capillary radius of the liquid–vapor interface in an MHP is comparable to the hydraulic diameter of the flow passage, and the capillary action dominates the gravitational force in the microchannel array. The capillary limit of an MHP thus depends on the capillary performance of the microchannel.

Several studies on capillary-driven flow have investigated the capillary performance of microchannels [21-40]. It has been found that the capillary force can be increased by decreasing the characteristic length, i.e., the hydraulic diameter, of the microchannel grooves [25-30], and controlling the surface structure [31-34] or wettability [35-37]. However, the pressure drop due to viscous friction in microchannels increases with the decreasing hydraulic diameter of the flow passage. Yang et al. reported that capillary filling of a nanochannel significantly degrades the performance [38]. Conversely, given the relatively high surface-to-volume ratio of a microchannel, the surface effect increases with the decreasing scale of the channel [41-44]. Nagayama et al. posited that the scale effect of the solid–liquid interfacial resistance in a microchannel becomes more significant with a decreasing hydraulic diameter [44]. The deviation from the classical theory with a decreasing hydraulic diameter is due to a breakdown of the continuum

solid–liquid boundary condition. In addition, the hydraulic and thermal resistances are the dominant causative factors of the poor thermal performance of microchannels. Optimization of the groove size is thus crucial to enhancing the thermal performance of a flat MHP.

In the present study, we developed a novel grooved converging microchannel array for a flat MHP to enhance the thermal performance [45]. To effectively draw the condensed working fluid back into the evaporation section of the microchannel, the hydraulic diameter of the grooves in the condensation section was made larger than that of the grooves in the evaporation section. The optimal groove size was determined based on the balance between the capillary and frictional forces in the rectangular grooves, taking into consideration the effect of surface wettability. Experiments were performed to compare the maximum input heat of the optimized converging microchannel with that of a straight microchannel. The heat pipe with the optimized converging microchannel was confirmed to exhibit a higher thermal performance. Experiments were also performed to clarify the effect of convergence on the force of the capillary-driven flow at room temperature and atmospheric pressure.

2. Theoretical model

Figure 1 shows a schematic of the open rectangular groove considered in this study. The groove height H and length L are constant, whereas the width $W(x)$ linearly decreases in the x-direction. The groove has a converging shape, with the cross-sectional area decreasing in the axial direction between the condensation and evaporation sections.

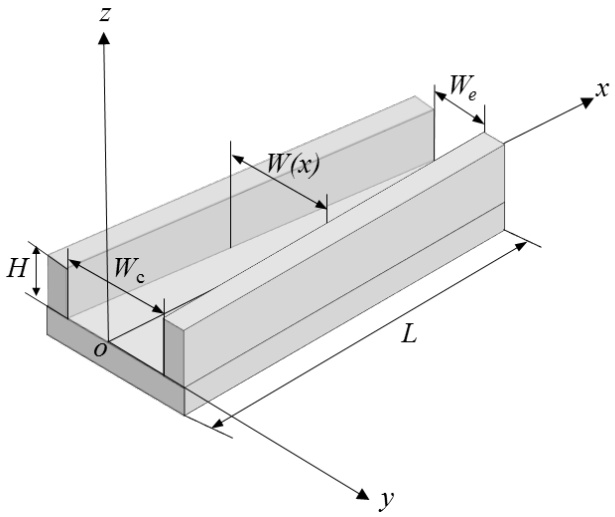

Figure 1 Model of a groove in the converging microchannel array for a flat MHP.

To optimize the groove size of the flat heat pipe, the balance between the capillary force and the pressure loss of the flow along the x-axis of the microchannel was derived based on the following assumptions:

(1) steady-state incompressible flow,

(2) saturated vapor,

(3) negligible heat generation due to viscous dissipation,

(4) no dry-out in the evaporation section, and

(5) no blocking in the condensation section.

The local physical properties of the liquid and vapor along the x-axis were considered temperature-dependent variables.

2.1 Capillary force

When a meniscus is formed at the liquid–vapor interface inside the groove, the local pressure difference at the interface at x, $\Delta p_i(x)$, can be calculated by the well-known Young–Laplace equation:

$$\Delta p_i(x) = \Delta p_v(x) - \Delta p_l(x) = \sigma_l(x)\cos\theta \cdot \left(\frac{1}{W(x)/2} + \frac{1}{H}\right), \quad (1)$$

where $\sigma_l(x)$ is the local surface tension of the liquid, and θ is the local contact angle of the meniscus.

Because the groove height H and length L are constant, a decrease in the groove width would increase the capillary pressure, according to Eq. (1). To effectively draw the condensed working fluid back into the evaporation section, the minimum groove width should be the optimized value for the evaporation section, resulting in the maximization of Eq. (1), while the maximum width should be the optimized value for the condensation section. The local pressure differences at the liquid–vapor interfaces in the condensation and evaporation sections are respectively given by

$$\Delta p_i(0) = \sigma_c \cos\theta_c \cdot \left(\frac{W_c + 2H}{W_c H}\right) \quad (2)$$

and

$$\Delta p_i(L) = \sigma_e \cos\theta_e \cdot \left(\frac{W_e + 2H}{W_e H}\right), \quad (3)$$

where σ_c, θ_c, and W_c ($=W(0)$) are respectively the local surface tension, contact angle, and width of the condensation section, and σ_e, θ_e, and W_e ($=W(L)$) are the corresponding parameters of the evaporation section.

For the considered open rectangular groove shown in Fig. 1, the total capillary pressure difference between the evaporation and condensation sections is given by

$$\Delta p_{ca} = \Delta p_i(L) - \Delta p_i(0) = \sigma_e \cos\theta_e \cdot \left(\frac{1}{W_e/2} + \frac{1}{H} \right) - \sigma_c \cos\theta_c \cdot \left(\frac{1}{W_c/2} + \frac{1}{H} \right). \quad (4)$$

2.2 Pressure loss

According to the mass conservation law, in the steady state, the mass evaporation rate in the evaporation section is balanced by the mass flow rate of the condensed liquid through the groove. Therefore, the mass flow rate $\dot{m}$ through the groove can be obtained as follows:

$$\dot{m} = \frac{Q}{h_{fg}}, \quad (5)$$

where Q is the input heat transfer rate (i.e., the input power), and h_{fg} is the latent heat. The mean flow velocity through the groove, $\bar{u}$, is thus given by

$$\bar{u} = \frac{\dot{m}}{\rho_l HWN} = \frac{Q}{\rho_l HWNh_{fg}}, \quad (6)$$

where ρ_l is the density of the liquid, and N is the number of grooves. Assuming a one-dimensional laminar flow through the groove in the axial (x) direction, the pressure loss Δp_{loss} of the mass flow rate $\dot{m}$ over a distance L is given by

$$\Delta p_{loss} = \int_0^L \frac{12\mu(x)u(x)}{W(x)^2} dx, \quad (7)$$

where $\mu(x)$ is the local viscosity of the liquid, and $u(x)$ is the local flow velocity. Because the groove width $W(x)$ linearly decreases in the x-direction, where

$$W(x) = W_c - \frac{W_c - W_e}{L} x, \quad (8)$$

the mass conservation in the x-direction becomes

$$W(x)u(x) = W_e u_e . \tag{9}$$

Hence, Eq. (7) can be rewritten as follows:

$$\Delta p_{loss} = \int_0^L \frac{12\mu(x) W_e u_e}{\left(W_c - (W_c - W_e)\cdot x / L\right)^3} dx . \tag{10}$$

2.3 Driving force of capillary flow through groove

The total capillary pressure change along the groove, Δp_{ca}, can be determined using Eq. (4), and the pressure loss Δp_{loss} over the distance L can be determined using Eq. (10). Further, the driving force of the capillary flow can be estimated from the difference between Δp_{ca} and Δp_{loss}, i.e., $\Delta p = \Delta p_{ca} - \Delta p_{loss}$. A positive driving force is required to draw the condensed liquid from the condensation section back into the evaporation section.

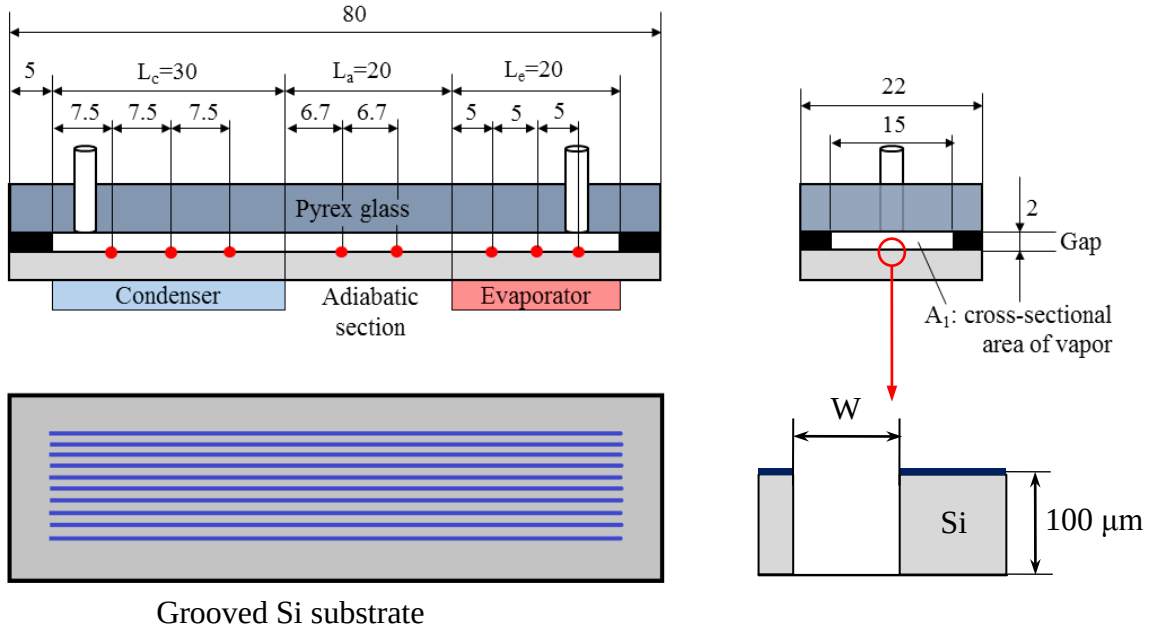

Figure 2 Test section of Si-based MHP.

3. Experimental method

3.1 Test section of flat MHP

Figure 2 shows the test section of the flat MHP fabricated on a P-type silicon wafer. The micro-electro-mechanical fabrication technique was employed for the fabrication. The grooves were etched on a 15 × 70 mm area on the Si substrate, which measured 22 × 80 mm. The height of all the grooves was set to 100±5 μm. The groove widths were determined using the theoretical predictions shown in the later section 4.1 based on the method described in the previous section. Table 1 gives the parameters for the considered experimental cases under an operating condition of T_c = 20 °C, T_e = 80 °C, θ_c = 80°, θ_e = 0°, H = 100 μm, L = 70 mm and Q = 20 W, as a demonstration for comparisons. The grooves of cases 1-4 had the rectangular cross section shown in Fig. 2 and were fabricated by Bosch deep reactive ion etching. A thin SiO_2 layer was deposited on the surface of the grooves by thermal oxidation. Separate chemical treatments were used to control the surface wettability of the evaporation section, adiabatic section, and condensation section. As indicated in Table 1, the surfaces of the evaporation and adiabatic sections were hydrophilic, while the surface of the condensation section was more hydrophobic than those of the evaporation and adiabatic sections, having a contact angle of approximately 80^o.

The grooved Si substrate was bonded to a Pyrex glass by a sandwiched silicone rubber sheet of

Table 1 Parameters of the grooves fabricated on Si substrates.

Cases	W_c [μm]	W_e [μm]	H [μm]	N	Contact angles [deg.]		
					θ_e, θ_a	θ_c*	θ_c**
1	300	100	100	42	0	80	0
2	400	200	100	33	0	82	0
3	300	300	100	33	0	80	0
4	100	100	100	50	0	80	0

*For heat pipe experiments. **For capillary-driven flow experiments.

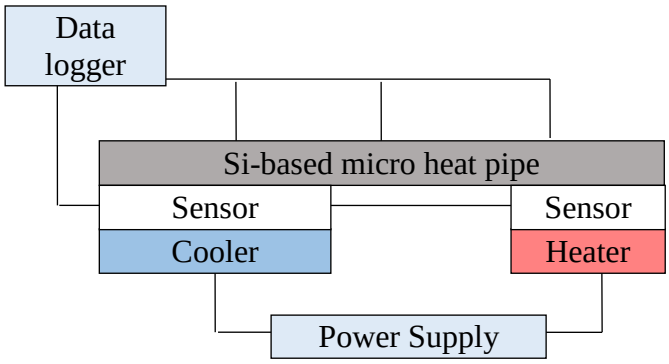

Figure 3 Experimental setup of MHP.

thickness 2 mm, as shown in Fig. 2. Two holes drilled into the Pyrex glass were used to evacuate the MHP and fill the working fluid into the MHP. Eight T-type thermocouples (diameter 0.2 mm, indicated by the red dots in Fig. 2) were used to measure the surface temperature of the grooved Si substrate. The lengths of the condensation, adiabatic, and evaporation sections of the MHP were 30, 20, and 20 mm, respectively. After fabrication, the MHP was evacuated to remove non-condensable gases, and then filled with ultra-pure water (Kishida Chemical, electrical resistivity 18 MΩ·cm) as the working fluid. The MHP was heated and part of the generated vapor was removed to attain a filling ratio of 50% [8].

3.2 Experimental setup of MHP

All the experiments were performed with the MHP oriented horizontally in a room at a constant temperature of 25 °C and constant humidity of 40 RH%. Figure 3 shows the experimental setup used to evaluate the thermal performance of the MHP. The evaporator and condenser were respectively heated and cooled using a flat heater and cooler. The heat flux supplied to the evaporator and condenser was measured using 0.4-mm-thick heat flux sensors (Captec, HF series). The thermal data were collected by a computer via a data logger. Thermal resistance of the heat pipe R_{hp}, mainly depending on summation of the evaporator resistance and the condensation resistance, can be written as follows [47]:

$$R_{hp} = \frac{1}{h_e A_e} + \frac{1}{h_c A_c}, \tag{11}$$

where h_e and h_c are the heat transfer coefficient of the evaporator and condenser, and A_e and A_c are the heat transfer area of the evaporator and condenser. Since the total wall resistances R_0 can be measured under the condition of the heat pipe without the working fluid, the overall thermal resistance of the flat heat pipe R_{total} can be obtained based on the thermal resistance network of R_{hp} and R_0 in parallel. Hence, the overall thermal resistance R_{total} becomes,

$$R_{total} = \frac{1}{\frac{1}{R_{hp}} + \frac{1}{R_0}} = \frac{T_e - T_c}{Q_{in}}, \tag{12}$$

where Q_{in} is the input heat and T_e-T_c is the overall temperature difference between the evaporator and condenser. Therefore, the thermal performance of the MHP can be characterized by the effective thermal conductivity λ_{hp} as follows,

$$\lambda_{hp} = \frac{L}{R_{hp} A_1} \tag{13}$$

where L is the length of the heat pipe and A_1 is the cross-sectional area of the vapor.

An uncertainty analysis has been performed according to the method proposed by Holman [46]. The estimated uncertainties of temperature is ±0.11 K (±0.16 %) for the thermocouples. The maximum value of uncertainty of the heat flux and the effective thermal conductivity, is 1.47 kW/m^2 (2.12 %) and 1.58 W/(m·K) (0.21 %) respectively.

3.3 Experiment on capillary-driven flow in open microchannel

A schematic of the capillary-driven flow is shown in Fig. 4 to clarify how the convergence increases the capillary force. The flow was observed by a motion analysis microscope (Keyence, VW-6000) on a horizontal stage at room temperature and pressure. The fabricated Si substrates were carefully cleaned with a mixture of sulfuric acid and hydrogen peroxide to obtain uniformly hydrophilic surfaces. A 6-μl ultra-pure water droplet was deposited on the Si substrate using a syringe. Once the droplet touched the hydrophilic substrate, the liquid began to flow through the groove under the action of the capillary force. A high-speed camera mounted on the motion analysis microscope was used to obtain images of

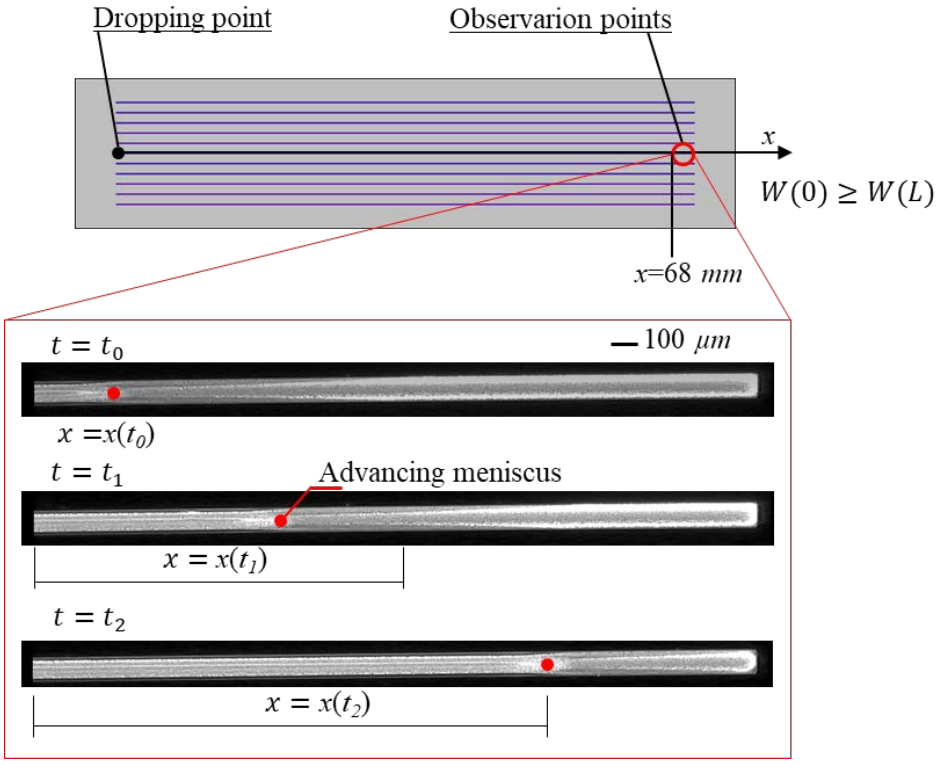

Figure 4 Schematic of the capillary-driven flow experiment setup and microscope images obtained at the observation point.

the liquid flow at the observation point located at x = 68 mm. Samples of the obtained images are shown in Fig. 4. A sharply concave advancing meniscus was observed, and the velocity of its inflection point (red dots in Fig. 4) was analyzed based on the time history of the flow images. The measurements for each experimental case were repeated more than 5 times to calculate the mean imbibition velocity.

4. Results and discussion

4.1 Theoretically determined optimal groove size

Figures 5 and 6 show the estimated force balance as a function of the groove width under an operating condition defined by T_c = 20 °C, T_e = 80 °C, θ_c = 80°, θ_e = 0°, H = 100 μm, L = 70 mm, and Q = 20 W. The total capillary pressure difference along the groove, Δp_{ca}, was calculated using Eq. (4), while the pressure loss Δp_{loss} over a distance L was calculated using Eq. (10). The driving force of the capillary flow was estimated from the difference between Δp_{ca} and Δp_{loss}, i.e., $\Delta p = \Delta p_{ca} - \Delta p_{loss}$.

For the straight groove, it is clear from Fig. 5 that decreasing the width increases both the capillary force and frictional force, with the driving force vanishing when the width is decreased to 50 μm. The peak driving force occurs at a groove width of approximately 100 μm. This width was thus considered as the optimal value under the above-specified operating condition.

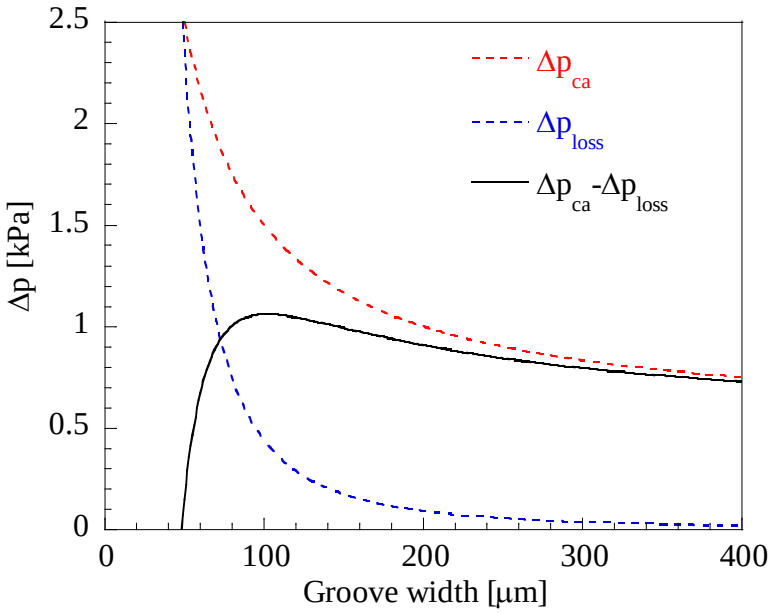

Figure 5 Effect of the groove width on the force balance in the straight groove for T_c = 20 °C, T_e = 80 °C, θ_c = 80°, θ_e = 0°, H = 100 μm, L = 70 mm, and Q = 20 W.

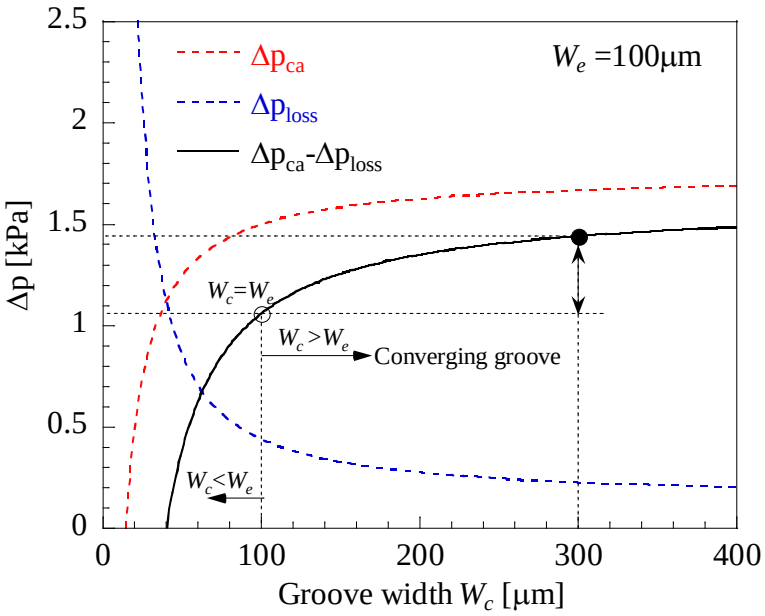

Figure 6 Effect of the groove width W_c and W_e on the force balance in the converging ($W_c > W_e$) or diverging ($W_c < W_e$) groove at T_c = 20 °C, T_e = 80 °C, θ_c = 80°, θ_e = 0°, H = 100 μm, L = 70 mm, and Q = 20 W for W_e = 100 μm.

Using the determined optimal width of the evaporation section in the converging groove, W_e = 100 μm, the driving force was obtained as a function of the groove width in the condensation section, W_c. Strictly speaking, the groove is divergent when $W_c < W_e$ and convergent when $W_c > W_e$. As can be observed from Fig. 6, for a constant W_e = 100 μm, the capillary force decreases with decreasing W_c owing to the increasing pressure loss, eventually vanishing at W_c = 40 μm. Compared to the straight groove (open circle in Fig. 6), the driving force of the converging groove is large for $W_c > W_e$, whereas it is small for $W_c < W_e$. This indicates that the enhancement of the driving force is only achieved in a converging groove. Considering the relatively small increase in the capillary and driving forces for W_c > 300 μm, 300 μm is considered to be the optimal value of W_c for a converging groove with W_e = 100 μm. The driving force in the converging groove with W_c = 300 μm and W_e = 100 μm is approximately 1.36 times that of the straight groove with a uniform width W = 100 μm.

Theoretically, decreasing the groove width in the evaporator section or increasing the groove width in the condenser section can increase the capillary performance than that with the optimized converging microchannels of 300μm -100μm. However, the solid-liquid interfacial resistance in a microchannel becomes significant with a decreasing hydraulic diameter and the thermal resistance are the dominant causative factor of the poor thermal performance of microchannels [44]. The thermal slip length (Kapitz length) is about 150μm for the bare Si surface, and about 80μm for the super-hydrophilic Si surface [48]. Thus, as a demonstration on the thermal performance of MHP with converging microchannels, the optimal groove width of straight microchannel of 100μm was used to the minimum groove width at the evaporator of MHP with converging microchannels in the present study.

4.2 Thermal performance of flat MHP

The temperature profiles for the different grooved Si surfaces are shown in Fig. 7 for the steady-state heat pipe operating condition defined by T_c = 20 °C and $T_e \leq$ 80 °C. The maximum temperature difference on the grooved surfaces was determined to be approximately 60 °C, with the temperature in the evaporation section increasing with increasing input heating power. Here, the maximum input heat was defined as the input heat when the operating temperature exceeded the temperature limit of 100 °C at the evaporator, which was indicated by the red symbols in Fig. 7. The maximum input heat for case 1 (converging microchannel with the optimized groove) was the highest among all the experimental cases, being 1.20 times that of case 2 (converging microchannel with the unoptimized groove), 1.64 times that of case 3 (straight microchannel with the unoptimized groove) and 1.21 times that of case 4 (straight microchannel with the optimized groove). For the same number of grooves (cases 2 and 3), the maximum input heat of case 2 (converging microchannel) is higher than that of case 3 (straight microchannel). Comparing the straight microchannels of cases 3 and 4, we found that case 4 with the smaller groove width and the larger number of the grooves has the higher maximum input heat. On the other hand, since the area of the evaporator is same for all the experimental cases, increasing the number of grooves will increase both the real heat transfer area and the liquid-vapor phase change area.

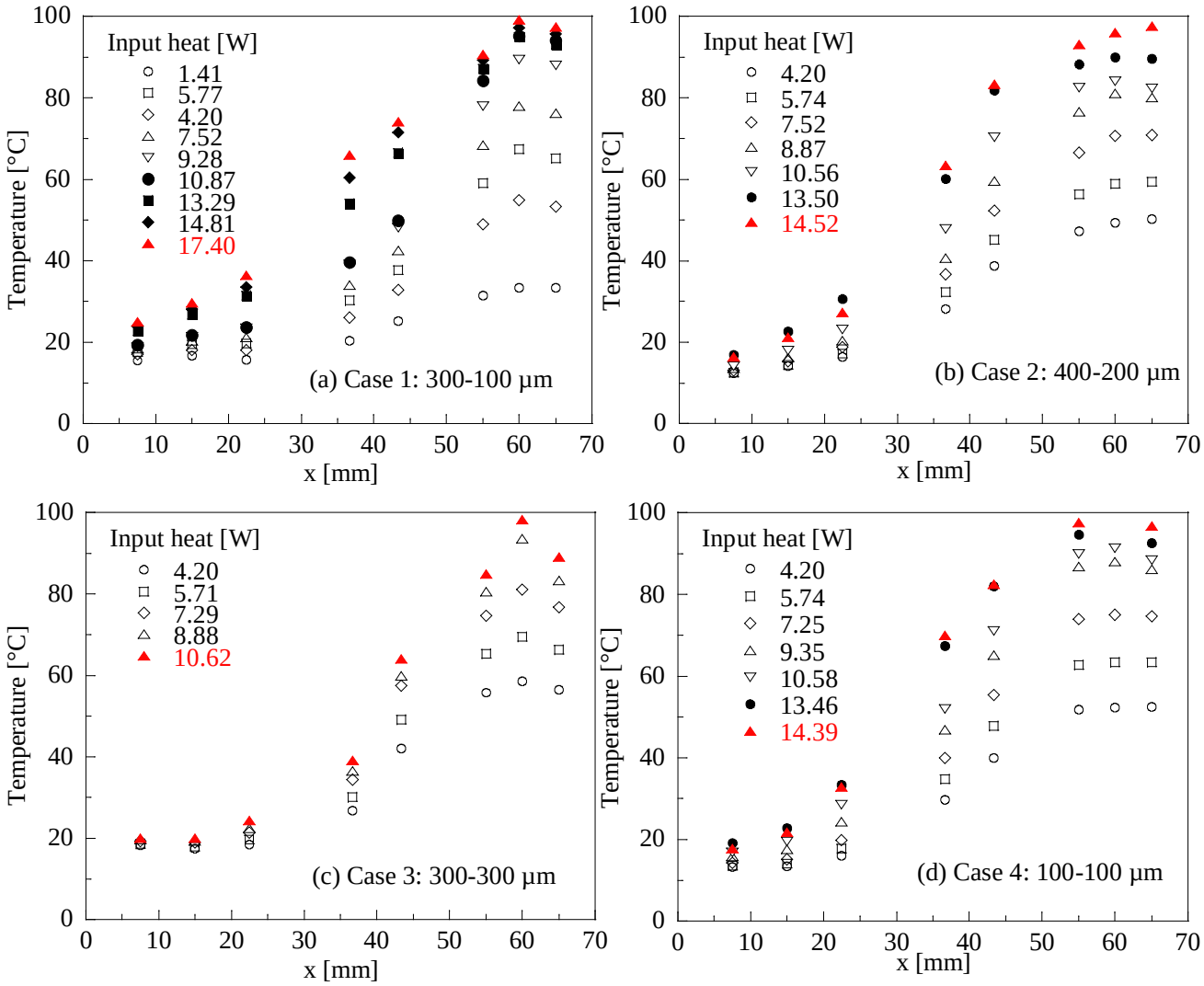

Figure 7 Temperature profiles of the fabricated flat MHPs: (a) case 1: converging MHP with the optimized groove; (b) case 2: converging MHP with the unoptimized groove; (c) case 3: straight MHP, and (d) case 4: optimized straight MHP.

However, the thermal performance of case 1 still was the highest of the other cases, although the groove number of case 1 is smaller than that of case 4. That is, the driving force obtained from the pressure difference plays primary role on the thermal performance of MHP; while the number of grooves (i.e. the real heat transfer area and the liquid-vapor phase change area) plays the secondary role. Thus, the MHP with the optimized converging microchannel was confirmed to exhibit better thermal performance than that with the straight microchannel.

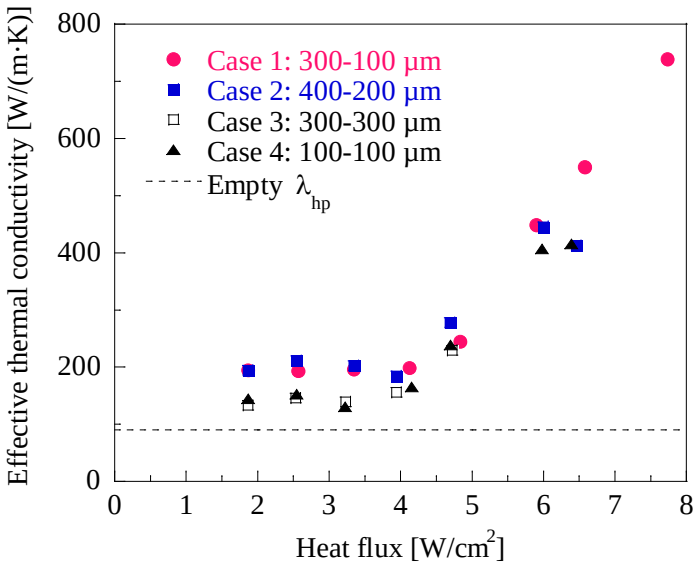

Figure 8 Effective thermal conductivities of the fabricated flat MHPs with respect to the heat flux.

Figure 8 shows the determined effective thermal conductivities of the different fabricated flat MHPs with respect to the heat flux. As can be seen, the thermal conductivity increases with increasing heat flux, with case 1 (converging channel with the optimized groove) exhibiting the highest thermal conductivity, approximately eight times that of the empty heat pipe without the working fluid (represented by the dotted line).

4.3 Capillary performance of groove

The capillary-driven flow at room temperature and pressure was observed to clarify the effect of convergence on the capillary force. The motion of the inflection point of the advancing concave meniscus was analyzed. In the vicinity of the observation point x = 68 mm, the groove width was approximately 100 μm in cases 1 and 4, 200 μm in case 2, and 300 μm in case 3. Figure 9 (a) shows the time history of the travel distance for the inflection point of the advancing concave meniscus obtained from the flow images in the vicinity of the observation point. The mean imbibition velocity of 5 measurements was shown in Fig. 9 (b). Case 1 exhibited a better capillary performance than cases 2, 3 and 4, substantiating the advantage of convergence for enhancing the capillary performance. Reduction of the groove width was thus found to improve the capillary performance, consistent with the observations of previous study [25]. However, this is inconsistent with the observations in

nanochannels [38]. Further studies are planed to investigate this difference between microscale and nanoscale grooves [49].

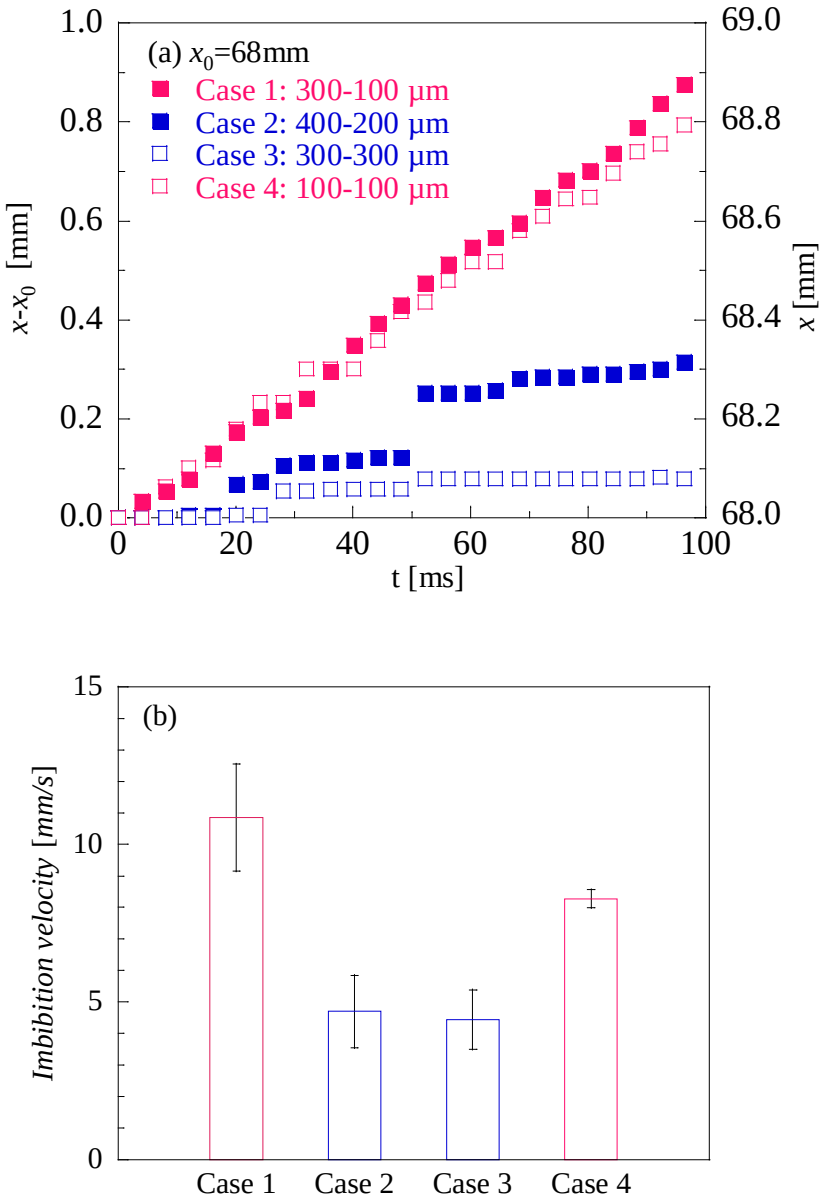

Figure 9 Capillary flow in microchannels observed at x = 68 mm: (a) typical time history of travel distance for the inflection point of the advancing concave meniscus; (b) mean imbibition velocity of the capillary flow.

5. Conclusion

We developed a novel grooved converging microchannel array for a flat MHP. The optimal groove size was estimated based on the balance between the capillary and frictional forces in the rectangular grooves, taking surface wettability into consideration. For a given operating condition of a 70-mm-long flat, converging MHP, defined by a condenser temperature of 20 °C, an evaporator temperature of 80 °C, and input heat of 20 W, the optimal groove widths were theoretically determined to be 100 μm in the hydrophilic evaporator section and 300 μm in the hydrophobic condenser section. Our experiments verified the theoretical estimates, and demonstrated that the MHP with the converging microchannel provides better thermal and capillary performance than that with a straight microchannel.

It is verified that the driving force from the pressure difference plays primary role on the thermal performance of MHP; however, the real heat transfer area and the liquid-vapor phase change area also plays the secondary role which cannot be ignored in the case of those significant decreasing at the evaporator section. On the other hand, as a demonstration on the thermal performance of MHP with converging microchannels, the optimal groove width of straight microchannel of 100μm was used to the minimum groove width at the evaporator of MHP with converging microchannels in the present study. Further investigations for the groove width less than 100μm with converging microchannles, as well as the scale effect of the solid-liquid interfacial resistance on thermal performance of MHP are expected in the future.

Acknowledgments

The micro-electro-mechanical fabrication of the micro heat pipes used in this study was partly supported by the Kitakyushu Foundation for the Advancement of Industry Science and Technology, and Yamaguchi University.

References

[1] J. Qu. Jian, H. Wu, P. Cheng, Q. Wang, Q. Sun, Recent advances in MEMS-based micro heat pipes, International Journal of Heat and Mass Transfer 110 (2017) 294-313.

[2] X. Chen, H. Ye, X. Fan, T. Ren, G. Zhang, A review of small heat pipes for electronics, Applied Thermal Engineering 96 (2016) 1-17.

[3] J. Li, L. C. Lv, Experimental studies on a novel thin flat heat pipe heat spreader, Applied Thermal Engineering 93 (2016) 139-146.

[4] A. J. Jiao, H.B. Ma, J.K. Critser, Evaporation heat transfer characteristics of a grooved heat pipe with micro-trapezoidal grooves, International Journal of Heat and Mass Transfer 50 (2007) 2905-2911.

[5] S.J. Kim, J.K. Seo, K.H. Do, Analytical and experimental investigation on the operational characteristics and the thermal optimization of a miniature heat pipe with a grooved wick structure, International Journal of Heat and Mass Transfer 42 (2003) 3405-3418.

[6] K.H. Do, S.J. Kim, S.V. Garimella, A mathematical model for analyzing the thermal characteristics of a flat micro heat pipe with a grooved wick, International Journal of Heat and Mass Transfer 51 (2008) 4637-4650.

[7] K.H. Do, S.P. Jang, Effect of nanofluids on the thermal performance of a flat micro heat pipe with a rectangular grooved wick, International Journal of Heat and Mass Transfer 53 (2010) 2183-2192.

[8] Y.J. Youn, S.J. Kim, Fabrication and evaluation of a silicon-based micro pulsating heat spreader, Sensors and Actuators A 174 (2012) 189-197.

[9] J. Qu, H. Wu, P. Cheng, Effects of functional surface on performance of a micro heat pipe, International Communications in Heat and Mass Transfer 35 (2008) 523-528.

[10] S. Launay, V. Sartre, M. Lallemand, Experimental study on silicon micro-heat pipe arrays, Applied Thermal Engineering 24 (2004) 233-243.

[11] Y.M. Hung, K.K. Tio, Thermal analysis of a water-filled micro heat pipe with phase-change interfacial resistance, ASME Journal of Heat Transfer 134 (2012) 112901-1-11.

[12] F. Lefèvre, M. Lallemand, Coupled thermal and hydrodynamic models of flat micro heat pipes for the cooling of multiple electronic components, International Journal of Heat and Mass Transfer 49 (2006) 1375-1383.

[13] R. Rullie`re, F. Lefe`vre, M. Lallemand, Prediction of the maximum heat transfer capability of two-phase heat spreaders–Experimental validation, International Journal of Heat and Mass Transfer 50 (2007) 1255-1262.

[14] F. Lefèvre, R. Rullière, G. Pandraud, M. Lallemand, Prediction of the temperature field in flat plate heat pipes with micro-grooves–Experimental validation, International Journal of Heat and Mass Transfer 51 (2008) 4083-4094.

[15] S. Lips, F. Lefèvre, J. Bonjour, Nucleate boiling in a flat grooved heat pipe, International Journal of Thermal Sciences 48 (2009) 1273-1278.

[16] R. Revellin, R. Rullière, F. Lefèvre, J. Bonjour, Experimental validation of an analytic model for predicting the thermal and hydrodynamic capabilities of flat micro heat pipes, Applied Thermal Engineering 29 (2009) 1114-1122.

[17] F. Lefèvre, R. Rullière, S. Lips, J. Bonjour, Confocal microscopy applied to capillary film measurements in a radial flat plate heat pipe made of silicon, Journal of Heat Transfer, 132 (2010) 031502-1-6.

[18] R. Shirakashi, I. Hagiya, S. Nishio, Study on high performance evaporator with micro grooves (Measurement of capillary force in single groove and modelling of heat and mass transfer), Transactions of JSME 74 (2008) 2190-2197.

[19] D. Hanazawa, T. Okawa, A study on phase change heat removal technique using a porous-microchannel, Transactions of JSME 81 (2015) 15-36.

[20] X. Wang, L. Zou, J. Liu, Y. Luo, G. Liu, B. Yu, Experimental investigation of copper-grooved micro heat pipes (MHPs), Journal of Solid State Lighting 1 (1) (2014) 1-8.

[21] P. Wu, H. Zhang, A. Nikolov, D. Wasan, Rise of the main meniscus in rectangular capillaries: Experiments and modeling, Journal of Colloid and Interface Science 461 (2016) 195-202.

[22] N. Fries, M. Dreyer, The transition from inertial to viscous flow in capillary rise, Journal of Colloid and Interface Science 327 (2008) 125-128.

[23] K. Li, D. Zhang, H. Bian, C. Meng, Y. Yang, Criteria for applying the Lucas–Washburn law, Science Reports 5 (2015) 14085.

[24] C.W. Extrand, Forces, pressures and energies associated with liquid rising in nonuniform capillary tubes, Journal of Colloid and Interface Science 450 (2015) 135-140.

[25] D. Yang, M. Krasowska, C. Priest, M.N. Popescu, J. Ralston, Dynamics of capillary driven flow in open microchannels, The Journal of Physical Chemistry C 115 (38) (2011) 18761-18769.

[26] N. Ichikawa, K. Hosokawa, R. Maeda, Interface motion of capillary-driven flow in rectangular microchannel, Journal of Colloid and Interface Science 280 (2004) 155-164.

[27] G. Lu, X. D Wang, Y. Y Duan, Study on initial stage of capillary rise dynamics, Colloids and Surfaces A 433 (2013) 95-103.

[28] F.F. Ouali, G. McHale, H. Javed, C. Trabi, N.J. Shirtcliffe, M.I. Newton, Wetting considerations in capillary rise and imbibition in closed square tubes and open rectangular cross-section channels, Microfluidics and Nanofluidics 15 (2013) 309-326.

[29] A. Hamraoui, T. Nylander, Analytical approach for the Lucas–Washburn equation, Journal of Colloid and Interface Science 250 (2002) 415-421.

[30] V.S. Duryodhan, A. Singh, S.G. Singh, A. Agrawal, Convective heat transfer in diverging and converging microchannels, International Journal of Heat and Mass Transfer 80 (2015) 424-438.

[31] M.M. Rahman, E. Ölçerog˘lu, M. McCarthy, Role of wickability on the critical heat flux of structured superhydrophilic surfaces, Langmuir 30 (2014) 11225-11234.

[32] M. Hasegawa, Forced wetting of microstructured surfaces, Journal of Fluid Science and Technology 9 (1) 13-00301 (2014) 1-9.

[33] B. Chan, J.K. Sung, Study on the capillary performance of micro-post wicks with non-homogeneous configurations, International Journal of Heat and Mass Transfer 68 (2014) 415-421.

[34] Y. Chen, L.S. Melvin, S. Rodriguez, D. Bell, M.M. Weislogel, Capillary driven flow in micro scale surface structures, Microelectronic Engineering 86 (2009) 1317-1320.

[35] T.D Blake, J.D. Coninck, The influence of pore wettability on the dynamics of imbibition and drainage, Colloids and Surfaces A 250 (2004) 395-402.

[36] V. Jokinen, S. Franssila, Capillarity in microfluidic channels with hydrophilic and hydrophobic walls, Microfluidics and Nanofluidics 5 (2008) 443-448.

[37] B. Jean-Cristophe, M.J.D. Michael, H. Stephan, S. Ralf, Transport dynamics in open microfluidic grooves, Langmuir 23 (9) (2007) 5200-5204.

[38] M. Yang, B.Y. Cao, W. Wang, H.M. Yun, B.M. Chen, Experimental study on capillary filling in nanochannels, Chemical Physics Letters 662 (2016) 137-140.

[39] R. Lucas, On the time law of the capillary rise of liquids, Kolloid-Z 23 (1918) 15-22.

[40] E.W. Washburn, The dynamics of capillary flow, Physical Review 17 (3) (1921) 273-283.

[41] G. Nagayama, M. Kawagoe, A. Tokunaga, T. Tsuruta, On the evaporation rate of ultra-thin liquid film at the nanostructured surface: a molecular dynamics study. International Journal of Thermal Sciences 49 (2010) 59-66.

[42] G. Nagayama, P. Cheng, Effects of interface wettability on microscale flow by molecular dynamics simulation, International Journal of Heat and Mass Transfer 47 (2004) 501-513.

[43] G. Nagayama, Boundary conditions and microscale heat transfer at solid-liquid interface, Journal of the Heat Transfer Society of Japan 50 (2011) 29-36.

[44] G. Nagayama, T. Matsumoto, K. Fukushima, T. Tsuruta, Scale effect of slip boundary condition at solid-liquid interface, Science Reports 7, 43125 (2017) 1-8.

[45] G. Nagayama, Japan Patent No. JP2015-127534, 2015.

[46] J, P Holman, Experimental methods for engineers 7th ed, McGraw-Hill, 2001.

[47] Japan Association for Heat Pipe, Jitsuyou Heat Pipe, Nikkan Kogyo Shimbun, Ltd., Tokyo, Japan, 1985.

[48] K. Fukushima, R. Mitoma, T. Tsuruta, G. Nagayama, Effect of Wettability on Solid-liquid Interfacial Resistance in Microchannel Flow, in: Proceedings of 16th International Heat Transfer Conference, Beijing, 10-15 August 2018, No. 23856.

[49] Y. Itahana, S. Gyotoku, T. Tsuruta, G. Nagayama, Capillary-driven Flow in Open Converging Microchannels, in: Proceedings of 16th International Heat Transfer Conference, Beijing, 10-15 August 2018, No. 22886.